



CHORUS

This is the accepted manuscript made available via CHORUS. The article has been published as:

Theory of dissociative recombination of molecular ions with competing direct and indirect mechanisms applied to CH^+

Xianwu Jiang, Josh Forer, Chi Hong Yuen, Mehdi Ayouz, and Viatcheslav Kokoouline

Phys. Rev. A **104**, 042801 — Published 4 October 2021

DOI: [10.1103/PhysRevA.104.042801](https://doi.org/10.1103/PhysRevA.104.042801)

Theory of dissociative recombination of molecular ions with competing direct and indirect mechanisms applied to CH^+

Xianwu Jiang^{1,*}, Josh Forer², Chi Hong Yuen^{2,†}, Mehdi Ayouz^{1,‡} and Viatcheslav Kokoouline²
¹*Université Paris-Saclay, CentraleSupélec, Laboratoire LGPM, Gif-sur-Yvette, France*
²*Department of Physics, University of Central Florida, Florida, USA*

(Dated: September 10, 2021)

This study presents a theoretical approach to model the dissociative recombination (DR) of molecular ions in which direct and indirect mechanisms are competing with each other. This is often the case for the ions having low-energy electronic resonances, such as open-shell molecular ions. The approach combines the UK R-matrix method for fixed-nuclei electron-ion scattering, the vibronic frame transformation with outgoing-wave dissociative functions obtained using a complex absorbing potential, and molecular quantum-defect theory. The present first-principles approach is applied to the CH^+ ion. The contribution of the Rydberg series converging to the two lowest excited electronic states of the ion, $a^3\Pi$ and $A^1\Pi$, plays a significant role in the DR cross section. The obtained DR cross section is in good agreement with experimental measurements at energies between 0.3 and 3 eV, but is much higher for energies below 0.3 eV. The disagreement is probably due to the rotational structure neglected in the present theory. The nature of prominent resonances in the computed results is analyzed by considering DR probabilities for different partial waves of the incident electron. It was found that the d -type partial waves ($d\sigma$ and $d\pi$) contribute considerably to the DR of CH^+ in its ground vibronic state.

I. INTRODUCTION

Dissociative recombination (DR) of molecular ions with electrons plays an important role in molecular plasma for a wide interval of temperatures with many applications: from a few K for the plasma in the interstellar medium to a few electron-volts, $10^4 - 10^5$ K, in technological processes such as plasma etching. Theory is now able to describe quite well the process for diatomic and small polyatomic ions with closed electronic shells. However, for the ions with an open shell, which, although short-lived, are often key intermediate species in non-equilibrium plasma, theory is not satisfactory.

Since the formulation of the first theoretical approach to model the process, given by Bardsley [1–3], one distinguishes two DR mechanisms, direct and indirect, and correspondingly two categories of molecular ions. The first category of ions are those in which the potential energy surface (PES) of a neutral state crosses the PES of the ground ionic state. Direct DR is generally dominant for these ions. The multichannel quantum-defect theory (MQDT) method, based on the treatment initially suggested by Giusti-Suzor [2] and later developed by several other authors, has shown to be the most successful way to describe the DR for such systems (e.g., N_2^+ [4], O_2^+ [5], NO^+ [6, 7], CO^+ [8], BF^+ [9], CF^+ [10], BeH^+ [11, 12], SH^+ [13], OH^+ [14], CH^+ [15–18]). To apply the approach, one typically needs the PES of the ground electronic state of the ion and wave functions of vibrational

levels in the PES, the PES of the dissociative states of the neutral molecule crossing the ionic surface in the Franck-Condon region, electronic couplings between the neutral dissociative states and the Rydberg series converging to the ground ionic state, and geometry-dependent quantum defects of the considered Rydberg states. For a DR calculation including multiple ionic states, the Rydberg-Rydberg couplings between different ionization channels are also needed.

The second category of ions are those in which no crossing occurs between the PES of the ground electronic state of the ion and the neutral-state PES in the Franck-Condon region. In this case, the DR proceeds through Rydberg states closed for dissociation via one or several neutral states open for dissociation. This is the indirect DR mechanism. The theory that was successful for the direct DR cannot be applied immediately to this situation.

Greene and collaborators [19–25] have suggested an efficient way to model the indirect DR process using the multichannel quantum-defect theory combined with the vibrational frame transformation involving not only wave functions of bound vibrational levels of the ion, but also wave functions of the dissociative continuum. Siegert pseudostates [19–21] and states obtained with a complex absorbing potential (CAP) [22, 26] were employed in the approach to represent outgoing dissociation flux. Compared to the Siegert pseudostates [27], CAP eigenstates obey a simpler orthonormality relationship and can be used in a situation with several coupled dissociative channels, such as in Refs. [22, 26].

For DR of molecular ions with low-lying electronically excited states, Mezei, Schneider, and collaborators (see [4, 16–18] and references therein) have developed a method based on a diabatic quantum-defect matrix. In this method, quantum defects depending on the internu-

*Department of Physics, Wuhan University of Technology, Wuhan 430074, China

†Department of Physics, Kansas State University, Manhattan, Kansas USA

‡Electronic address: mehdi.ayouz@centralesupelec.fr

clear distance R are derived from energies of excited Rydberg states of the neutral molecule. Due to the presence of several ionic states, the Rydberg series are coupled to each other, producing multiple avoided crossings in the derived quantum defects as functions of R . To remove the strong R -dependence of the quantum defects, a diabaticization procedure is applied, which produces a smooth diabatic matrix of quantum defects. The diabaticization step is very laborious, not unique, and sometimes not accurate because numerous Rydberg states are involved (see Fig. 1 in Ref. [4]). The approach becomes impractical for polyatomic ions. This is a significant limitation of an otherwise very efficient DR method.

In Ref. [28], we have suggested a different MQDT-based approach to describe collisions between an electron and a molecular ion, and applied it to study vibronic excitations of CH^+ . The three lowest electronic states of CH^+ were included in the treatment. Couplings between Rydberg series produced by the three electronic states are accounted for in the energy-dependent scattering matrix of the $\text{CH}^+ + e^-$ system, which is constructed by the MQDT closed-channel elimination procedure. In this study, we extend the approach to model the DR process in $\text{CH}^+ + e^-$ collisions. For the $\text{CH}^+ + e^-$ system, a neutral-state resonance PES crosses the PES of the CH^+ ground electronic state just slightly to the left from the Franck-Condon region, so that direct and indirect DR mechanisms are expected to be competing and contributing to the total DR cross sections. This approach is based on the idea that the above-mentioned resonance state crossing the ionic PES has a Rydberg character and, therefore, can be represented by the MQDT electronic closed-channel elimination procedure. The electronic coupling between the initial continuum-state of electron-ion system and the resonance state can thus also be accounted for in the scattering matrix by the elimination procedure. In other words, we can treat the direct (through the resonance PES) and indirect (through other more excited Rydberg states) mechanisms in the same framework.

This paper is organized in the following way. A brief review of previous theoretical and experimental studies of the low-energy DR of CH^+ is given in the next section. In Sections III and IV, we present how electronic and vibrational states of the $\text{CH}^+ + e^-$ system are described in our theoretical approach. Section V discusses the construction of the scattering matrix for $\text{CH}^+ + e^-$ collisions. Section VI gives formulas for the calculation of the DR cross section. Section VII is devoted to obtained results and Section VIII is the conclusion.

II. PREVIOUS STUDIES OF THE DISSOCIATIVE RECOMBINATION OF CH^+

The DR of CH^+ has been studied theoretically and experimentally in several works. The process is the main destructive mechanism of CH^+ in the interstellar

medium, leading to the formation of complex interstellar molecules, especially polyatomic hydrocarbons. Having accurate DR cross sections for the process is important for a reconciliation of calculated and observed abundances of interstellar CH^+ .

In early studies, Bardsley and Junker [29], as well as Krauss and Julienne [30], calculated the adiabatic PESes of CH and CH^+ . They found that the PES of the repulsive “ $^2\Pi(3)$ ” state of CH (see Fig. 1 of Ref. [29]) intersects the PES of the ground electronic state of CH^+ near the equilibrium internuclear distance. CH in the “ $^2\Pi(3)$ ” state formed in a low-energy $\text{CH}^+ + e^-$ collision would finally dissociate to $\text{C}(^1D) + \text{H}(^2S)$ through a coupling to the “ $^2\Pi(2)$ ” state by the avoided crossing (see Fig. 1 of Ref. [29]). Both groups found a large DR rate constant, with a lower bound of $10^{-7} \text{ cm}^3/\text{s}$ at 100 K. Based on these results, calculated equilibrium intensity of interstellar CH^+ in the steady-state chemistry model of Smith, Liszt, and Lutz [31] was over 100 times smaller than observed. A few years later, Giusti-Suzor and Lefebvre-Brion [32] found a considerably lower DR rate. They considered Rydberg-type orbitals in the PES calculations of CH . The resulting PESes showed no crossing between the $^2\Pi$ dissociative state and the ionic ground state. A better agreement between the predictions and measurements could be deduced with this smaller DR rate.

The larger values of the theoretical DR rate constant were consistent with the experimental value of about $3 \times 10^{-7} \text{ cm}^3/\text{s}$ at 120 K measured with a merged electron-ion beam method [33, 34]. The remaining controversy between the experiment and the results of Ref. [32] was carefully investigated by Takagi *et al.* [15], who have improved the model used by Giusti-Suzor and Lefebvre-Brion [32] and combined it with a complete DR theory developed by Giusti [2]. The diabatic PES of a neutral $^2\Pi$ state was found to cross the ionic PES at $R = 1.832$ bohrs, in the Franck-Condon region. The DR cross sections and rate constant were accurately computed, not estimated, as in earlier studies, for the first time. The obtained results agreed with the experimental measurements [33] within a factor of 1.2-2, depending on the energy. The theoretical results were limited to collision energies below 0.3 eV.

With an improved heavy ion storage-ring technique, a detailed experimental study of the DR for fully relaxed CH^+ was carried out by Amitay *et al.* in 1996 [35]. The measured DR cross section agrees with previous measurements and has a better resolution showing a number of resonances. The large DR cross section was again attributed to the crossing between the $^2\Pi$ dissociative state of CH and the ionic ground state. Broad resonance structures were present in the DR cross sections. Considering the low-lying excited states of CH^+ , the resonances were assigned to the core-excited Rydberg states.

To identify the observed broad resonances, Carata *et al.* [16] performed an elaborate MQDT modeling of the DR of CH^+ . The Rydberg series converging to the $X^1\Sigma^+$ ground electronic state and to the next two excited states

($a^3\Pi$ and $A^1\Pi$) of the ion were included in the treatment. The overall shape and main features of the obtained DR cross section at low energies (< 4 eV) agree with the experimental results by Amitay *et al.* [35]. However, the overall magnitude of the theoretical cross section was smaller by a factor of 2-10 for energies below 0.3 eV. The disagreement was attributed to the neglected contributions from (a) the d -type partial waves and (b) $^2\Sigma^+$ resonances. Chakrabarti *et al.* [17] recently performed a similar MQDT calculation, in which two excited electronic states of the ion were accounted for. However, similar to the study of Carata *et al.* [16], the only symmetry of the $\text{CH}^+ + e^-$ system included in the treatment was $^2\Pi$ and the d partial wave was neglected. The inclusion of the excited ionic states added the indirect mechanism to the treatment and increased the theoretical cross section, approaching it to the experimental values. However, positions of major resonances in the theoretical cross section disagree significantly with the experiment. Later, the rotationally resolved DR cross section, without accounting for the excited ionic states, was considered by the same team [18]. Good agreement with the experiment was found for energies below 0.15 eV, while at higher energies the theoretical cross section is significantly smaller than in the experiment.

III. ELECTRONIC MODEL

PEs of the three lowest electronic states of CH^+ and the $^2\Pi$ dissociative (resonance) state of CH are shown in Fig. 1. The PES of the $^2\Pi$ resonance state crosses that of the $X^1\Sigma^+$ ground ionic state near the left turning point of the first excited vibrational state [36].

Being the main path for direct DR, the $^2\Pi$ resonance contributes significantly to the DR cross section. However, the indirect process may not be negligible, at least, for certain collision energies. The indirect process can proceed through highly excited Rydberg states of the $^2\Pi$ symmetry, but also through other symmetries, which were completely neglected in previous theoretical studies. In our recent study of vibrational excitation of CH^+ [28], we suggested a method to include the $^2\Pi$ resonance and all other Rydberg states of CH in the description of electron-ion scattering using the same uniform MQDT-based approach. The approach will also be used in the present study; below, we discuss it only briefly.

The main electronic configuration of the $^2\Pi$ resonance state is $1\sigma^2 2\sigma^2 3\sigma 1\pi 4\sigma$, which corresponds to the following atomic orbitals at large internuclear distances: $3\sigma \rightarrow 1s_{\text{H}}$, $1\pi \rightarrow 2p_{\text{C}}$, and $4\sigma \rightarrow 2p_{\text{C}}$. The 4σ orbital has a Rydberg character at small internuclear distances. This character is caused by the coupling between the $3\sigma 1\pi(^1\Pi)4\sigma$ and $3\sigma 1\pi(^3\Pi)4\sigma$ states of CH , i.e., the incident electron in the 4σ Rydberg orbital plus the $a^3\Pi$ and $A^1\Pi$ states of CH^+ . The $^2\Pi$ resonance state together with the excited $a^3\Pi$ and $A^1\Pi$ states are therefore included in the present MQDT description of the $e^- + \text{CH}^+$

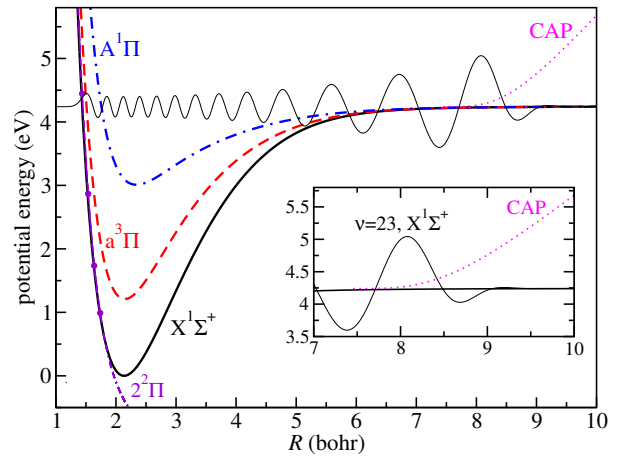


FIG. 1: The PEs of the three lowest electronic states: $X^1\Sigma^+$ (black solid curve), $a^3\Pi$ (red dashed curve), and $A^1\Pi$ (blue dot-dashed curve). The violet (dot-double-dashed) curve shows the PES of the $^2\Pi$ resonance state: circles are obtained in the R-matrix calculations, the line in the bound-state region is the PES from Ref. [17]. Also, the imaginary part of the CAP (see the text) is drawn with a magenta dotted curve. The inset shows an enlarged view of the CAP (imaginary part) and vibrational function $v = 23$ of the $X^1\Sigma^+$ state to demonstrate the effect of CAP absorption.

system, as it was done in Ref. [28].

In this study, fixed-nuclei R-matrix calculations are performed, and the resulting 3×3 energy-independent scattering matrix is selected according to the procedure described in Ref. [28]. Therein, more details on the calculations can be found in Section V.

The two excited electronic states of the ion are closed to ionization at low scattering energies. Therefore, the low-energy $^2\Pi$ resonance state of Rydberg character could be accounted for using the MQDT electronic closed-channel elimination procedure. The elimination procedure is performed using the 3×3 electronic scattering matrices of $^2\Pi$ symmetry selected above the $A^1\Pi$ threshold. Figure 2 compares the low-energy resonance obtained at $R=1.337$, 1.437 , and 1.537 bohrs using two methods: the closed-channel elimination procedure (dashed line) and the direct R-matrix scattering calculations (solid lines). Obtained energies of the resonance are listed in Table I. No resonance is found at $R=1.837$ bohrs. At this internuclear distance, the resonance PES goes below the ground state of the ion.

As one can see, the energies of the resonance reproduced by the channel elimination are shifted to the left, and the widths are slightly narrower than those in the R-matrix calculations. The difference in energies and widths of the resonance, obtained by the two methods, is attributed to the energy dependence of coupling elements in the reactance (and scattering) matrix. The inter-channel couplings in the matrix obtained in the channel-elimination procedure are the same as in the matrix taken at energies above the $A^1\Pi$ threshold, while the couplings

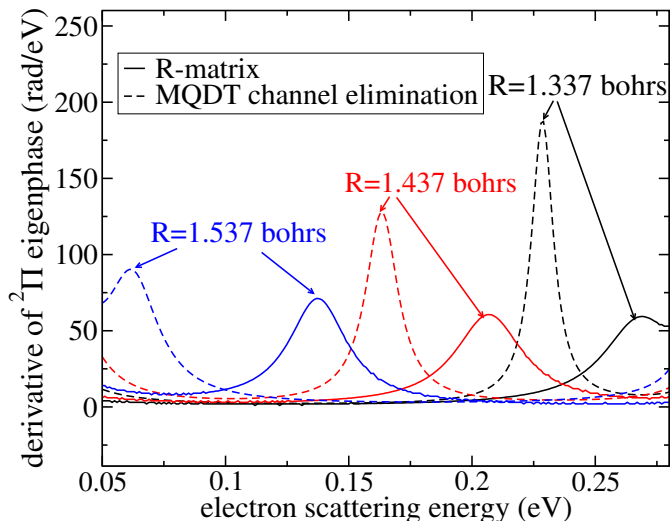


FIG. 2: The figure demonstrates derivatives of the eigenphase sum for the $^2\Pi$ symmetry, which are used to derive energies and widths of the resonance. Results from the R-matrix calculations are shown by solid curves and the results from the MQDT channel elimination by dashed curves. The results are shown for three different values of R : 1.337, 1.437, and 1.537 bohrs. Details of the R-matrix calculations can be found Section V of Ref. [28].

in the R-matrix calculations vary with energy. The effect is more important for smaller distances, such $R=1.337$ and 1.437 bohrs (see Fig. 2), for which the widths obtained by the two methods are different by almost a factor of two. At these geometries, the energy at which the reactance matrix is evaluated (above the $A^1\Pi$ threshold) is much larger than the energy of the resonance (see Fig. 1). At larger values of R , such as 1.537 bohrs, the energy of the $A^1\Pi$ threshold is lower, and the differences in the inter-channel couplings and the widths of the resonance, obtained by the two methods, are smaller (see Fig. 2). Therefore, in the Franck-Condon region of the ground vibrational level of the $X^1\Sigma^+$ state, the two methods are expected to produce almost the same reactance and scattering matrices.

TABLE I: Energies (in eV) of the low-energy $2^2\Pi$ resonance obtained in the R-matrix calculations and in the channel elimination procedure for different internuclear distances R (in bohrs).

R	R-matrix	Channel elimination
1.137	0.388	0.253
1.237	0.336	0.247
1.337	0.269	0.230
1.437	0.207	0.166
1.537	0.139	0.064
1.637	0.061	0.036
1.737	0.042	0.020
1.837	-	-

An important result of the above discussion is that the energy-independent scattering matrix with the $X^1\Sigma^+$, $a^3\Pi$, and $A^1\Pi$ electronic states is able to represent the $2^2\Pi$ dissociative state when the MQDT electronic closed-channel elimination procedure is applied.

IV. VIBRONIC STATES

The dissociation proceeds through a number of excited vibronic Rydberg states of CH, which are bound with respect to dissociation. To describe the dissociation, the vibrational continuum states of the CH molecule should be accounted for. In our theoretical model, the vibrational bound and continuum states are represented using a uniform approach. For this purpose the vibrational continuum of each electronic state, $X^1\Sigma^+$, $a^3\Pi$, and $A^1\Pi$, of the ion is discretized using a CAP, which was constructed in a manner similar to that in Ref. [26]. Wave functions of the vibrational levels with energies above the corresponding dissociation energy have outgoing-wave boundary conditions. Vibrational energies of such states are complex. The vibrational states (bound and discretized continuum) generate a vibrational basis, which is used in the DR treatment as it was developed in Refs. [19–21, 26].

This study implements the CAP method in the following way. Energies and wave functions of vibrational states are obtained in a separate (non-coupled) calculation for each of the three electronic states, $X^1\Sigma^+$, $a^3\Pi$, and $A^1\Pi$, numerated by index i . For each electronic state $|i\rangle$, the vibrational Schrödinger equation is solved by adding a purely imaginary potential to the corresponding PES, $V_i(R)$, at the end of interval along the internuclear distance R . The vibrational Hamiltonian is then

$$\hat{H} = -\frac{\hbar^2}{2m} \frac{d^2}{dR^2} + V_i(R) - i\eta W(R), \quad (1)$$

where η is the CAP strength and $W(R)$ is a potential function of the form [37]

$$W(R) = \begin{cases} N \exp\left(-\frac{2L}{R-R_0}\right) & \text{for } R > R_0, \\ 0 & \text{for } R < R_0, \end{cases} \quad (2)$$

N is a constant with a value of 13.22 [37], L is the CAP length, and R_0 is the starting point of the CAP. PESes and the CAP are displayed in Fig. 1. In Eq. (1) m is the reduced mass of the C and H atoms.

The eigenenergies ϵ_{iv} and eigenfunctions ϕ_{iv} of the Hamiltonian in Eq. (1) are obtained by a discrete variable representation method [38]. The matrix of the above Hamiltonian in the discrete variable representation is not Hermitian, but complex symmetric, so that eigenenergies are, in general, complex

$$\epsilon_{iv} = E_{iv} - i\frac{\Gamma}{2}, \quad (3)$$

where E_{iv} is the energy of the vibrational state and Γ is the width of the state, if the energy E_{iv} is above the dissociation threshold $V_i(R \rightarrow \infty)$. Otherwise (for bound

vibrational states), Γ is negligible. The set of obtained vibrational wave functions $\phi_{iv}(R)$, together with the electronic part $|i\rangle$ of the total wave functions, forms a vibronic basis and obeys the orthonormality relationship

$$\langle i', \phi_{i'v'} | i, \phi_{iv} \rangle = \delta_{i'i} \int \phi_{i'v'}(R) \phi_{iv}(R) dR = \delta_{i'v',iv}, \quad (4)$$

where the vibrational functions in the integral are not complex conjugated.

The CAP parameters, the damping strength η and length $L - R_0$ of the CAP, are chosen according to Ref. [37]. The CAP should be placed away from the main well of the PESes of CH^+ . $L = 10$ bohrs and $R_0 = 7$ bohrs are used for the three electronic states in this study. Using Eq. (20) and Table VI of Ref. [37], η was chosen to be 3×10^{-2} atomic units. The imaginary part of the CAP is shown in the inset of Fig. 1. The absorption of a dissociative vibrational state ($v = 23$, $X^1\Sigma^+$) by the CAP is also demonstrated in the figure.

V. SCATTERING MATRIX

The reactance matrix (K-matrix) for a given internuclear distance R is computed using the UK R-matrix codes [39] and Quantemol-N suite [40] in the C_{2v} point group in the basis of real spherical harmonics. In this study, we transform the basis to the one with complex spherical harmonics, which are better adapted for the natural symmetry group $C_{\infty v}$ of CH^+ .

First, channel functions of the incident electron are transformed from real $Y_{l,\lambda}$ to complex Y_l^λ spherical harmonics according to

$$\begin{pmatrix} Y_l^\lambda \\ Y_l^{-\lambda} \end{pmatrix} = \frac{1}{\sqrt{2}} \begin{pmatrix} (-1)^\lambda & i(-1)^\lambda \\ 1 & -i \end{pmatrix} \begin{pmatrix} Y_{l,\lambda} \\ Y_{l,-\lambda} \end{pmatrix}, \quad (5)$$

where λ is assumed to be positive and $Y_{l,\lambda} = Y_l^\lambda$ if $\lambda = 0$. The real spherical harmonics $Y_{l,\lambda}$ depend on the azimuthal angle ϕ as $\cos(\lambda\phi)$, while $Y_{l,-\lambda} \sim \sin(\lambda\phi)$. In the C_{2v} group, the real spherical harmonics $Y_{l,\lambda}$ transforms as the A_1 irreducible representation (irrep) if λ is even, and the B_1 irrep if λ is odd. The harmonics $Y_{l,-\lambda}$ transforms as the A_2 irrep for even λ and the B_2 irrep for odd λ .

Real-valued two-component channel functions of the $a^3\Pi$ and $A^1\Pi$ states of the ion transform as B_1 and B_2 irreps in C_{2v} . We will use notations $A^1\Pi_{B_1}$ and $A^1\Pi_{B_2}$ (similarly, $a^3\Pi_{B_1}$ and $a^3\Pi_{B_2}$) for the two-component channel functions. They also need to be transformed to have projections of the electronic angular momentum of a definite sign. The relative phase of the two components B_1 and B_2 is arbitrary, so we choose the same phase convention as in the above transformation: the transformation to complex-valued channel functions Π^\pm with a definite sign of the projection of the angular momentum on the molecular axis is given by

$$\begin{pmatrix} \Pi^+ \\ \Pi^- \end{pmatrix} = \frac{1}{\sqrt{2}} \begin{pmatrix} -1 & -i \\ 1 & -i \end{pmatrix} \begin{pmatrix} \Pi_{B_1} \\ \Pi_{B_2} \end{pmatrix}, \quad (6)$$

for each pair of the $a^3\Pi$ and $A^1\Pi$ states. The transformation matrix of Eq. (6) is the same as Eq. (5) with $\lambda = 1$.

Applying the unitary transformations of the incident-electron channel functions (Eq. (5)) and the electronic states of the target molecule (Eq. (6)) produces a set of channels with definite projections (and of a definite sign) of the total angular momentum of the $\text{CH}^+ + e^-$ system on the molecular axis. The reactance $K(R)$ and scattering $S(R)$ matrices are block-diagonal with respect to the total projection of the angular momentum.

All R -dependent matrices ($K(R)$, $S(R)$, $\Delta(R)$), discussed below and written in the basis of complex-valued channel functions, have the same set of channel indexes. Each channel is numerated by three quantum numbers: i refers to one of the five electronic states (including the degeneracy) of the target ion ($X^1\Sigma^+$, $a^3\Pi^\pm$, $A^1\Pi^\pm$), l and λ are the angular momentum and its projection on the molecular axis of incident electron. In our calculation, we included partial waves with $l = 0 - 4$, which makes the size of the partial-wave space to be 25. Accounting for five (in the C_{2v} group) electronic states of the ion, included in the treatment, makes the total number of channels to be 125.

To compute the DR cross section, we need the scattering matrix in the basis of vibronic channels. Such a matrix is obtained by the vibrational frame transformation. Ideally, for this procedure, we need the $K(R)$ -matrix calculated for a relatively large number of internuclear distances R to be able to accurately represent its R -dependence. However, due to a strong R -dependence of $K(R)$, especially near the equilibrium geometry of CH^+ , and the arbitrary sign of target channels at different values of R , the matrix $K(R)$ obtained in the R-matrix calculation is not a smooth function of R . We decided to limit the R-matrix calculation only to the Franck-Condon region, corresponding to the ground vibrational level of the ion in the $X^1\Sigma^+$ state. Details of the procedure follow.

First, we transform the matrix $K(R)$ into the matrix of scattering phase shifts $\Delta(R)$ (phase matrix). Formally, the two matrices are related to each other by the expression

$$K(R) = \tan \Delta(R). \quad (7)$$

In practice, to obtain the matrix $\Delta(R)$, we find eigenvalues of $K(R)$ and its eigenvectors (that form the corresponding unitarity transformation) and evaluate the arctangent of eigenvalues to produce eigenvalues of $\Delta(R)$ (eigenphases). Then, the matrix $\Delta(R)$ is obtained from its eigenphases by the inverse unitarity transformation.

The advantage of the phase matrix over the K-matrix is that it does not diverge when one of the eigenphases approaches $\pm\pi/2$, i.e., the phase matrix could be used for interpolation along R even when the K-matrix diverges. In particular, the K-matrix diverges near the CH^+ equilibrium geometry, while $\Delta(R)$ is a near-linear function of R . This allows us to represent the R -dependent matrix

$\Delta(R)$ in the following form

$$\Delta^{\text{ext}}(R) = \Delta(R_1) + (R - R_1)\alpha, \quad (8)$$

where α is the matrix

$$\alpha = \frac{\Delta(R_2) - \Delta(R_1)}{R_2 - R_1}. \quad (9)$$

and matrices $\Delta(R_2)$ and $\Delta(R_1)$ are obtained from the R-matrix calculations performed at two values of the internuclear distances R_2 and R_1 near the CH^+ equilibrium geometry. Here, we used $R_1 = 2.127$ bohrs and $R_2 = 2.137$ bohrs. We also had to make sure that the relative sign of channels obtained in the R-matrix calculations is unchanged. This is needed to be able to use the linear dependence in Eq. (8).

Having the matrix $\Delta(R)$ allows us to obtain the scattering matrix $S(R)$. The two matrices are formally related by

$$S(R) = \exp(2i\Delta(R)). \quad (10)$$

As in Eq. (7), the expression above is evaluated using eigenvalues of the two matrices and the corresponding unitarity transformation.

Vibrational frame transformation is performed by the integral

$$S_{i'v'l'\lambda',ivl\lambda} = \int dR \phi_{i'v'}(R) S_{i'v'l'\lambda',ivl\lambda}(R) \phi_{iv}(R). \quad (11)$$

Notice that the vibrational wave functions in the integral are not complex conjugated.

The continuous variable R in the scattering matrix before the vibrational frame transformation is replaced with a discrete vibrational quantum number v , so that channels in the new scattering matrix are labelled with four quantum numbers: the electronic state of the target i , the vibrational quantum number v of the target, and the partial-wave quantum numbers l, λ of the incident electron. The energy E_{iv} of a particular channel $|ivl\lambda\rangle$ depends only on i and v .

VI. DISSOCIATIVE RECOMBINATION CROSS SECTION

The matrix of Eq. (11) in the representation of vibronic channels $|ivl\lambda\rangle$ describes the scattering when all the channels are open for ionization, i.e., the energy E_{tot} of the $\text{CH}^+ + e^-$ system is above the energy of the highest channel included in the treatment. When the total energy E_{tot} is below the energy of the highest channel, some channels are closed and the scattering matrix describing the situation is obtained from the one of Eq. (11) by the closed-channel elimination procedure [41, 42]. The energy E_{tot} determines whether a particular channel is energetically open ($E_{tot} > E_{iv}$) or closed ($E_{tot} < E_{iv}$).

If channels in the scattering matrix are ordered by increasing energy E_{iv} , open and closed channels at a given energy E_{tot} split the matrix of Eq. (11) into the blocks

$$S = \begin{pmatrix} S^{oo} & S^{oc} \\ S^{co} & S^{cc} \end{pmatrix}. \quad (12)$$

The scattering matrix $S^{phys}(E_{tot})$ describing the actual scattering at energy E_{tot} only has open channels and is obtained by the MQDT closed-channel elimination procedure [41] from the partition of Eq. (12)

$$S^{phys}(E_{tot}) = S^{oo} - S^{oc} [S^{cc} - e^{-2i\beta}]^{-1} S^{co}, \quad (13)$$

where β is the energy-dependent diagonal matrix with elements

$$\beta_{i'v',iv} = \frac{\pi}{\sqrt{2}(\epsilon_{iv} - E_{tot})} \delta_{i'v',iv}. \quad (14)$$

Energies in the above equation are in atomic units.

Energies ϵ_{iv} of dissociative channels, obtained using the CAP, are complex with negative imaginary part, which makes β to be complex with positive real and imaginary parts. As a result, the matrix of Eq. (13) becomes sub-unitary [19, 21, 22]. The loss of unitarity is associated with the possibility of the $\text{CH}^+ + e^-$ system to dissociate during the electron-ion collision.

Once the matrix $S^{phys}(E_{tot})$ is computed, the DR cross section for the CH^+ ion initially being in state $|iv\rangle$ is obtained from the unitarity defect of the scattering matrix by

$$\begin{aligned} \sigma_{iv}(E_{el}) &= \sum_{l\lambda} \sigma_{ivl\lambda}(E_{el}), \\ \sigma_{ivl\lambda}(E_{el}) &= \frac{\pi \hbar^2}{2m_e E_{el}} \left[1 - \sum_{i'v'l'\lambda'} |S_{i'v'l'\lambda',ivl\lambda}^{phys}(E_{tot})|^2 \right]. \end{aligned} \quad (15)$$

In the above expressions, the energy of the incident electron E_{el} is related to the energy of the initial state E_{iv} and the total energy E_{tot} of the system as $E_{tot} = E_{iv} + E_{el}$.

VII. RESULTS

The convergence of the computed results was tested by varying the number N_v of vibrational levels (including discretized dissociative states) used in the calculations, the starting point of the CAP R_0 , and the CAP damping strength η . Figure 3 shows the DR cross section for the ion initially in the ground vibronic level, obtained using four different sets of the parameters. The agreement between the four different calculations is good, which indicates that the computed cross sections are well converged. The set of parameters (1), shown in the figure, is used for the final calculations.

The computed total DR cross section starting from the ground vibronic state of CH^+ as well as the available experimental [35] and theoretical [15–18] results are

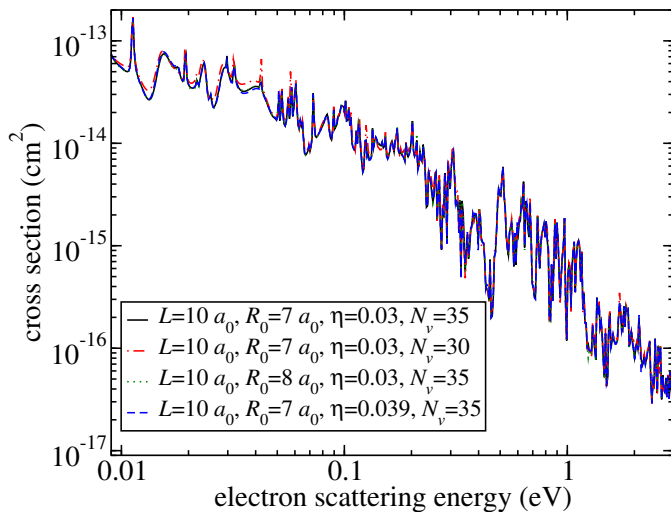


FIG. 3: The DR cross section for the ground vibronic state of CH^+ obtained with different sets of parameters of the computational model. The cross sections are computed using the following parameters: (1) $L = 10 a_0$, $R_0 = 7 a_0$, $\eta = 0.030$, $N_v = 35$ (solid), (2) $L = 10 a_0$, $R_0 = 7 a_0$, $\eta = 0.030$, $N_v = 30$ (red dot-dashed), (3) $L = 10 a_0$, $R_0 = 8 a_0$, $\eta = 0.030$, $N_v = 35$ (green dotted), (4) $L = 10 a_0$, $R_0 = 7 a_0$, $\eta = 0.039$, $N_v = 35$ (blue dashed), where N_v is the number of vibrational states for each electronic state.

displayed in Fig. 4. The focus of the study is the low-energy DR so that the collision energy E_{el} is restricted to be below 3 eV. In order to be able to compare with the available experimental data of Ref. [35], the non-Maxwell-Boltzmann distribution over collision velocities was accounted for as in previous studies (see, for example, Ref. [22]). In the present calculation, we used the uncertainty $E_{\parallel} = 0.5$ meV in the parallel contribution to the total energy and $E_{\perp} = 17$ meV in the transverse contribution. The values are taken from Ref. [35].

Arrows on the top axis of Fig. 4 mark the lowest vibronic ionization thresholds $v = 1 - 4$ of the $X^1\Sigma^+$ state and $v = 0$ of the $a^3\Pi$ state. Generally, the cross section decreases quite significantly when the scattering energy exceeds a threshold. Just below a given threshold, the incident electron can excite the target ion and be captured into a Rydberg state, thereby becoming attached to that excited state. Once the energy of the electron exceeds the threshold, the electron still excites the target, but now has enough kinetic energy to leave the excited ion. The probabilities of both excitation processes (just below and above the ionization threshold) are the same, but the overall DR probability is reduced when the total energy of the system is slightly above the threshold energy.

Numerous Rydberg resonances are present in the computed results. The majority of narrow resonances are produced due to capture of the incident electron into vibrationally excited Rydberg states attached to the elec-

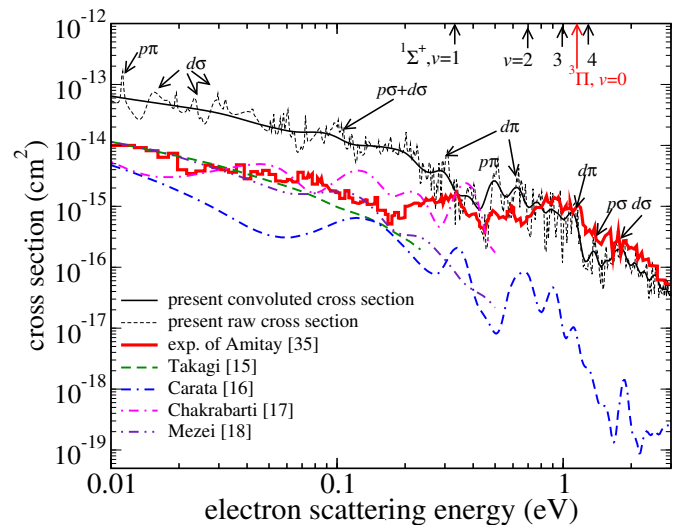


FIG. 4: The raw cross section obtained in this study (black thin dashed line) and the one convoluted with experimental uncertainties in the electron beam (black solid line) are compared with experimental measurements by Amitay *et al.* [35] (thick red solid line) and theoretical results by Takagi *et al.* [15] (green dashed line), Carata *et al.* [16] (blue dot-double-dashed line), Chakrabarti *et al.* [17] (magenta dot-dashed line), and Mezei *et al.* [18] (violet double-dot-dashed line). Labels of partial waves of the incident electron are assigned to prominent resonances (see Fig. 5). Several excited ionization thresholds ($v = 1 - 4$ of the $X^1\Sigma^+$ state and $v = 0$ of the $a^3\Pi$ state) are marked on the top of the figure.

tronic ground state of the ion. Wider resonances are produced by capturing the electron into the electronically-excited states, $a^3\Pi$ and $A^1\Pi$ [16, 35]. The two types (wide and narrow) of resonances are better seen in Fig. 5, which shows partial-wave contributions to the DR probability.

When the raw cross section is convoluted with the experimental uncertainties mentioned above, the narrow resonances are partially washed out. The Rydberg series in energy intervals approaching ionization thresholds produce relatively wide features with unresolved individual resonances. For example, the feature just below 0.3 eV is mainly produced by the Rydberg series converging to the $a^3\Pi, v = 1$ threshold, having the total $^2\Sigma$ symmetry. As clear from panel (c) of Fig. 5, the purely vibrational Rydberg series are modulated with wide vibronic resonances.

The computed DR cross section agrees well with the experimental data [35] for energies above 0.3 eV. The present theory is also able to reproduce all prominent experimental resonances, such as those situated at 0.08 eV, 0.3 eV, 0.5 eV, and 0.65 eV. However, there is a significant disagreement with the experiment at lower energies, below 0.3 eV. It is likely that the disagreement is due to the neglected rotational structure in the theoret-

ical approach. On the other hand, the good agreement between the theory and the experiment at energies >0.3 eV, where the electron can excite resonances attached to the $a^3\Pi$ and $A^1\Pi$ electronic states, indicates that the present treatment correctly describes couplings between the three electronic states included in the treatment. The conclusion is also supported by the observation that the previous theoretical studies, in which the excited electronic states of the ion were neglected [15, 16, 18] or treated using very modest data describing the couplings [17], produced much lower DR cross sections compared to the experiment. It means that inclusion of the excited electronic states is important to describe the DR process at energies above approx 0.2 eV.

The part in the square brackets of Eq. (15) could be regarded as the contribution $P_{ivl\lambda}$ of partial wave $l\lambda$ to the total the DR probability

$$P_{ivl\lambda}(E_{el}) = 1 - \sum_{i'v'l'\lambda'} |S_{i'v'l'\lambda',ivl\lambda}^{phys}(E_{el})|^2. \quad (16)$$

Figure 5 displays different contributions $P_{ivl\lambda}$ for the process starting from the ground state of CH^+ with $i = 1, v = 0$. Note that the partial waves with $\lambda \neq 0$ are doubly degenerate. As the figure demonstrates, at scattering energies below 0.04 eV, the dominant contribution is due to the $d\sigma$ partial wave, except the $p\pi$ resonance near 12 meV in panel (d). Prominent peaks occur near 0.016, 0.023, 0.029, 0.1, and 1.8 eV for the $d\sigma$ partial wave, near 0.011 and 0.5 eV for the $p\pi$ partial wave, and near 0.31, 0.64, and 1.21 eV for the $d\pi$ partial wave. The majority of the $d\sigma$ resonances in panel (c) are Rydberg states attached to the $v = 1$ vibrational level of the ground electronic state $X^1\Sigma^+$, situated near 0.3 eV above the lowest vibronic level. The $p\pi$ (as well as $d\pi$) resonances belong to Rydberg series attached to the excited electronic states of the ion.

VIII. CONCLUSIONS

As a summary, we would like to stress the following key findings of the present study.

- We described a theoretical method to compute cross sections for dissociative recombination of diatomic molecular ions having low-energy electronic resonances. The method combines techniques from several previous studies, developed for diatomic and polyatomic ions, with the method of obtaining couplings directly from electron-scattering calculations performed at fixed interatomic distances.
- Previously, only the group of Mezei and Schneider [16] was able to treat the dissociative recombination of the molecular ions, for which the direct and indirect DR mechanisms compete with each other. In all other theoretical DR studies, only one of the two mechanisms was treated at once. The method

described in this study is able to treat such situations with the two competing mechanisms in a uniform way.

- A significant advantage of the present method over the method of Ref. [16] is that the couplings between the ground and excited electronic states of the ion are obtained directly from the electron-scattering calculations, but not from energies of Rydberg bound states of the neutral molecule. No diabaticization and fitting procedure, like in Ref. [16, 17], is needed.
- The direct DR mechanism is treated using a different approach in the present method compared to Ref. [16]: There is no need in the present treatment to compute widths and energies of resonance curves crossing the ionic potential curve, like in the case of CH^+ , considered here. The electron capture and dissociation along one or several resonance curves are represented in a uniform way with indirect DR mechanisms.
- An important key ingredient of the present approach is the use of the dissociating vibrational states [19, 21] of the ions, used in the vibrational frame transformation.
- The developed method can be used to compute the DR cross sections for a large number of diatomic ions, which could not be treated previously due to complexity of electronic structure of the target ion and the corresponding neutral system. For instance, the method can be applied without modifications to molecular ions with an open electronic shell. The dominant mechanism in this case is, most likely, the direct mechanism and proceeds via one of several dissociative states crossing the ionic curve near the equilibrium geometry. Additionally, the method can be used to compute DR cross sections for ions in electronically excited states. For open-shell ions and ions in excited electronic states, experimental measurements of the cross sections are extremely difficult, if possible at all. Therefore, a theoretical approach is the only way to provide the corresponding data.
- We applied the developed theory to the DR of CH^+ . At $\text{CH}^+ + e^-$ collision energies above 0.3 eV, theory agrees well with the experiment. However, for lower energies, there is a significant disagreement, which is attributed to the rotational structure neglected in the present approach. The fact that the theory agrees with the experiment at energies above 0.3 eV and reproduces major resonances observed in the experimental DR spectrum suggests that the present theory describes the interaction of the excited states of the ion with the incident electron well.

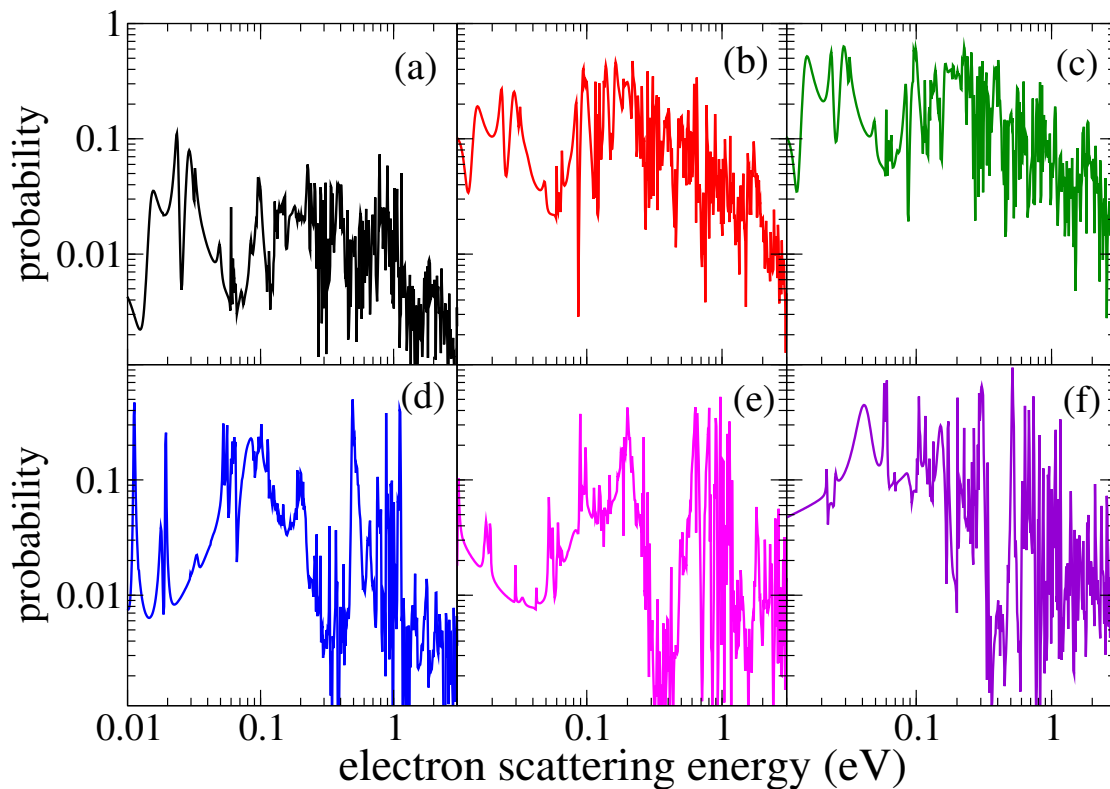


FIG. 5: Dominant partial wave contributions $P_{00l\lambda}$ (Eq. (16)) to the total DR probability of ion initially being in the ground vibronic state. (a) – $P_{00s\sigma}$, (b) – $P_{00p\sigma}$, (c) – $P_{00d\sigma}$, (d) – $P_{00p\pi}$, (e) – $P_{00d\pi}$, (f) – $P_{00d\delta}$.

- The method presented above does not account for the rotational structure of the target ion. The development accounting for the rotational structure is under way.

Acknowledgments

This work acknowledges the support from the National Science Foundation, Grant Nos. PHY-1806915 and PHY-

2102188, the Chinese Scholarship Council, the Thomas Jefferson Fund of the Office for Science and Technology of the Embassy of France in the United States, and the Fulbright U.S. Student Program. It has also received funding from the program “Accueil des chercheurs étrangers” of CentraleSupélec and “Séjour à l’étranger 2019” of école doctorale INTERFACES of Université Paris-Saclay. The authors are grateful to helpful discussions with Profs. Pietro Cortona from CentraleSupélec and Samantha Douguet from Rollins College.

-
- [1] J. Bardsley, *J. Phys. B* **1**, 365 (1968).
 [2] A. Giusti, *J. Phys. B* **13**, 3867 (1980).
 [3] A. Florescu-Mitchell and J. Mitchell, *Phys. Rep.* **430**, 277 (2006).
 [4] D. A. Little, K. Chakrabarti, J. Z. Mezei, I. F. Schneider, and J. Tennyson, *Phys. Rev. A* **90**, 052705 (2014).
 [5] S. L. Guberman, *Science* **278**, 1276 (1997).
 [6] I. Schneider, I. Rabadán, L. Carata, L. Andersen, A. Suzor-Weiner, and J. Tennyson, *J. Phys. B* **33**, 4849 (2000).
 [7] H. Sun and H. Nakamura, *J. Chem. Phys.* **93**, 6491 (1990).
 [8] J. Z. Mezei, R. Backodissa-Kiminou, D. Tudorache, V. Morel, K. Chakrabarti, O. Motapon, O. Dulieu, J. Robert, W.-Ü. L. Tchang-Brillet, A. Bultel, X. Urbain, J. Tennyson, K. Hassouni, and I. F. Schneider, *Plasma Sources Sci. Technol.* **24**, 035005 (2015).
 [9] J. Z. Mezei, F. Colboc, N. Pop, S. Ilie, K. Chakrabarti, S. Niyonzima, M. Lepers, A. Bultel, O. Dulieu, O. Motapon, J. Tennyson, K. Hassouni, and I. F. Schneider, *Plasma Sources Sci. Technol.* **25**, 055022 (2016).
 [10] O. Novotný, O. Motapon, M. H. Berg, D. Bing, H. Buhr, H. Fadil, M. Grieser, J. Hoffmann, A. Jaroshevich, B. Jordon-Thaden, C. Krantz, M. Lange, M. Lestinsky, M. Mendes, S. Novotny, D. A. Orlov, A. Petrigani, I. F. Schneider, A. Orel, and A. Wolf, *J. Phys. Conf. Ser.* **192**, 012021 (2009).

- [11] S. Niyonzima, N. Pop, F. Iacob, Å. Larson, A. Orel, J. Z. Mezei, K. Chakrabarti, V. Laporta, K. Hassouni, D. Benredjem, A. Bultel, J. Tennyson, D. Reiter, and I. F. Schneider, *Plasma Sources Sci. Technol.* **27**, 025015 (2018).
- [12] S. Niyonzima, S. Ilie, N. Pop, J. Z. Mezei, K. Chakrabarti, V. Morel, B. Peres, D. A. Little, K. Hassouni, A. Larson, A. E. Orel, D. Benredjem, A. Bultel, J. Tennyson, D. Reiter, and I. F. Schneider, *Atom. Data Nuc. Data* **115**, 287 (2017).
- [13] D. Kashinski, D. Talbi, A. Hickman, O. Di Nallo, F. Colboc, K. Chakrabarti, I. Schneider, and J. Z. Mezei, *J. Chem. Phys.* **146**, 204109 (2017).
- [14] S. L. Guberman, *J. Chem. Phys.* **102**, 1699 (1995).
- [15] H. Takagi, N. Kosugi, and M. Le Dourneuf, *J. Phys. B* **24**, 711 (1991).
- [16] L. Carata, A. E. Orel, M. Raoult, I. F. Schneider, and A. Suzor-Weiner, *Phys. Rev. A* **62**, 052711 (2000).
- [17] K. Chakrabarti, J. Z. Mezei, O. Motapon, A. Faure, O. Dulieu, K. Hassouni, and I. Schneider, *J. Phys. B* **51**, 104002 (2018).
- [18] Z. J. Mezei, M. D. Epée Epée, O. Motapon, and I. F. Schneider, *Atoms* **7**, 82 (2019).
- [19] E. L. Hamilton and C. H. Greene, *Phys. Rev. Lett.* **89**, 263003 (2002).
- [20] V. Kokoouline and C. H. Greene, *Phys. Rev. Lett.* **90**, 133201 (2003).
- [21] V. Kokoouline and C. H. Greene, *Phys. Rev. A* **68**, 012703 (2003).
- [22] S. Fonseca dos Santos, V. Kokoouline, and C. H. Greene, *J. Chem. Phys.* **127**, 124309 (2007).
- [23] R. Čurík and C. H. Greene, *J. Phys. Conf. Ser.* **115**, 012016 (2008).
- [24] D. J. Haxton and C. H. Greene, *Phys. Rev. A* **79**, 022701 (2009).
- [25] R. Čurík and C. H. Greene, *J. Chem. Phys.* **147**, 054307 (2017).
- [26] V. Kokoouline and C. H. Greene, *Phys. Rev. A* **72**, 022712 (2005).
- [27] O. I. Tolstikhin, V. N. Ostrovsky, and H. Nakamura, *Phys. Rev. A* **58**, 2077 (1998).
- [28] X. Jiang, C. H. Yuen, P. Cortona, M. Ayouz, and V. Kokoouline, *Phys. Rev. A* **100**, 062711 (2019).
- [29] J. Bardsley and B. Junker, *Astrophys. J.* **183**, L135 (1973).
- [30] M. Krauss and P. Julienne, *Astrophys. J.* **183**, L139 (1973).
- [31] W. H. Smith, L. S. Liszt, and B. L. Lutz, *Astrophys. J.* **183**, 69 (1973).
- [32] A. Giusti-Suzor and H. Lefebvre-Brion, *Astrophys. J.* **214**, L101 (1977).
- [33] J. Mitchell and J. W. McGowan, *Astrophys. J.* **222**, L77 (1978).
- [34] P. Mul, J. Mitchell, V. D'Angelo, P. Defrance, J. W. McGowan, and H. Froelich, *J. Phys. B* **14**, 1353 (1981).
- [35] Z. Amitay, D. Zajfman, P. Forck, U. Hechtfisher, B. Seidel, M. Grieser, D. Habs, R. Repnow, D. Schwalm, and A. Wolf, *Phys. Rev. A* **54**, 4032 (1996).
- [36] K. Chakrabarti, R. Ghosh, and B. Choudhury, *J. Phys. B* **52**, 105205 (2019).
- [37] A. Vibok and G. Balint-Kurti, *J. Phys. Chem.-US* **96**, 8712 (1992).
- [38] V. Kokoouline, O. Dulieu, R. Kosloff, and F. Masnou-Seeuws, *J. Chem. Phys.* **110**, 9865 (1999).
- [39] J. Tennyson, *Phys. Rep.* **491**, 29 (2010).
- [40] J. Tennyson, D. B. Brown, J. J. Munro, I. Rozum, H. N. Varambhia, and N. Vinci, *J. Phys. Conf. Ser.* **86**, 012001 (2007).
- [41] M. Seaton, *Rep. Prog. Phys.* **46**, 167 (1983).
- [42] M. Aymar, C. H. Greene, and E. Luc-Koenig, *Rev. Mod. Phys.* **68**, 1015 (1996).